THE JOURNAL OF BIOLOGICAL CHEMISTRY
Vol. 278, No. 35, Issue of August 29, pp. 33562–33570, 2003

Printed in U.S.A.

Assembly of Archaeal Cell Division Protein FtsZ and a GTPase-inactive Mutant into Double-stranded Filaments*

Received for publication, April 11, 2003, and in revised form, June 4, 2003
Published, JBC Papers in Press, June 14, 2003, DOI 10.1074/jbc.M303798200

María A. Oliva‡§, Sonia Huecas‡, Juan M. Palacios‡, Jaime Martín-Benito¶, José M. Valpuesta¶, and José M. Andreu‡‖

From the ‡Centro de Investigaciones Biológicas and the ¶Centro Nacional de Biotecnología, Consejo Superior de Investigaciones Científicas, E28006 Madrid, Spain

We have studied the assembly and GTPase of purified FtsZ from the hyperthermophilic archaeon *Methanococcus jannaschii*, a structural homolog of eukaryotic tubulin, employing wild-type FtsZ, FtsZ-His$_6$ (histidine-tagged FtsZ), and the new mutants FtsZ-W319Y and FtsZ-W319Y-His$_6$, with light scattering, nucleotide analyses, electron microscopy, and image processing methods. This has revealed novel properties of FtsZ. The GTPase of archaeal FtsZ polymers is suppressed in Na^+-containing buffer, generating stabilized structures that require GDP addition for disassembly. FtsZ assembly is polymorphic. Archaeal FtsZ(wt) assembles into associated and isolated filaments made of two parallel protofilaments with a 43 Å longitudinal spacing between monomers, and this structure is also observed in bacterial FtsZ from *Escherichia coli*. The His$_6$ extension facilitates the artificial formation of helical tubes and sheets. FtsZ-W319Y-His$_6$ is an inactivated GTPase whose assembly remains regulated by GTP and Mg^{2+}. It forms two-dimensional crystals made of symmetrical pairs of tubulin-like protofilaments, which associate in an antiparallel array (similarly to the known Ca^{2+}-induced sheets of FtsZ-His$_6$). In contrast to the lateral interactions of microtubule protofilaments, we propose that the primary assembly product of FtsZ is the double-stranded filament, one or several of which might form the dynamic Z ring during prokaryotic cell division.

Bacterial cells place at their division site a Z-ring that assembles from FtsZ at the cytosolic side of the plasma membrane and recruits the other protein components of the septation machinery. The positioning of the Z-ring is in turn determined by the self-organizing Min system (1–3). Archaeal FtsZ from *Methanococcus jannaschii* and eukaryotic tubulin share the same structural framework and constitute a distinct family of protofilament-forming GTPases (4, 5). The structures of bacterial FtsZs are probably similar to the archaeal protein, based on FtsZ sequence conservation. The *Escherichia coli* Z-ring is very dynamic, with turnover in seconds, similar to or faster than a typical mitotic spindle (6). Although the position of the Z ring was visualized by immunoelectron microscopy (7), its structure is unknown. A number of studies have shown that purified bacterial FtsZ can assemble with GTP and divalent cations forming polymers that hydrolyze the nucleotide β–γ phosphate bond and disassemble upon GTP consumption (8–13), although the mechanism linking GTP hydrolysis and exchange to the polymer dynamics (14) remains controversial (15–17). FtsZ polymers have the characteristic tubulin ~40 Å axial spacing between consecutive monomers (18). At pH 6 and in the presence of high Ca^{2+} and GTP concentrations, a small proportion of archaeal FtsZ from *M. jannaschii* formed crystalline sheets made of symmetric protofilament pairs associated in an antiparallel arrangement, whereas most of the protein precipitated into aggregates of helical cable-like tubes. Manual fitting of the structure of GDP-bound FtsZ from *M. jannaschii* (19) into a three-dimensional electron microscopy map of the sheet polymers has led to the current tubulin-like FtsZ protofilament model (5). Purified bacterial FtsZ without macromolecular additives or Ca^{2+} assembles into polymers apparently made of two or several protofilaments (9, 12, 16, 20, 21), although single-stranded segments can also be observed in negative stain, and employing scanning transmission electron microscopy, at low FtsZ concentrations single-stranded polymers have been reported (15).

FtsZ folding, activation, and assembly have important differences with tubulins. Purified unfolded FtsZ polypeptide chains are capable of spontaneous refolding into their functional states (21) in contrast to tubulin monomers, whose folding process includes binding and release from cytoplasmic chaperonin CCT (22). We have hypothesized that the extensive tubulin loop insertions in the FtsZ/tubulin common core and its folding complexity coevolved with the lateral association interfaces responsible for the association of parallel protofilaments into microtubules, suggesting that tubulin and FtsZ share a similar axial interaction between monomers, but have different interactions between protofilaments (21). Employing molecular dynamics it has been predicted that GTP binding controls the conformation of switch loop T3, which activates FtsZ for assembly possibly in a manner similar to tubulin (23). In this work we have investigated the assembly of archaeal FtsZ from *M. jannaschii*. We started by defining the conditions for biochemically regulated assembly of this FtsZ, and show that the GTPase of FtsZ is activated by polymerization, and that GDP induces disassembly. Subsequently, results not found before with other FtsZ proteins have provided new insight into FtsZ assembly. Archaeal FtsZ assembles without hydrolyzing GTP in sodium-containing buffer. The mutation W319Y also suppresses the GTPase activity of the archaeal FtsZ, generating stabilized polymers and two-dimensional crystals. Archaeal FtsZ assemblies are made of symmetrical pairs of tubulin-like protofilaments, which associate in a manner different than that of

* This work was supported by grants from MCyT BIO-1999-0859-c03-02 and BIO2002-03665, CAM 07B/0026/2002 (to J. M. A.), MCyT BMC2001-0950 (to J. M. V.), Programa de Grupos Estratégicos de la Comunidad de Madrid, and Red Temática de Investigación Cooperativa FIS C03/14 (CIB). The costs of publication of this article were defrayed in part by the payment of page charges. This article must therefore be hereby marked "*advertisement*" in accordance with 18 U.S.C. Section 1734 solely to indicate this fact.

§ Recipient of a predoctoral fellowship from FPI.

‖ To whom correspondence should be addressed: CIB, CSIC, Ramiro de Maeztu 9, 28020 Madrid, Spain. Fax: 34-91536042; E-mail: j.m.andreu@cib.csic.es.

tubulin. We propose that these double-stranded polymers constitute the primary assembly product of archaeal FtsZ and show that they are also formed in bacterial FtsZ from *E. coli*.

EXPERIMENTAL PROCEDURES

FtsZ, FtsZ-His$_6$, FtsZ-W319Y, and FtsZ-W319Y-His$_6$ Proteins—FtsZ-His$_6$ from *M. jannaschii,* which is wild-type FtsZ (FTSZ1) with a C-terminal Gly-Ser-His$_6$ extension, and its mutant FtsZ-W319Y-His$_6$, were overproduced in *E. coli* BL21(DE3)pLys transformed with the plasmid pHis17-mjFtsZ-H$_6$ (19, 24) or pAVK1(W319Y) (23), respectively, and purified by HiTrap Ni^{2+}-chelating affinity and size-exclusion chromatography as described (21, 23). The FtsZ-W319Y-His$_6$ mutant had been originally constructed as an intermediate step to the double mutant FtsZ-W319Y-T92W-His$_6$, whose single tryptophan fluorescence is sensitive to GDP or GTP binding (23). Plasmids coding for FtsZ and FtsZ-W319Y, both without the Gly-Ser-His$_6$ extension, were respectively constructed using the plasmids pHis17-mjFtsZ-H$_6$ or pAVK1(W319Y) as templates, by inverse PCR with the Expand High Fidelity PCR system (Roche Applied Science) in a GeneAmp PCR 2400 (PerkinElmer Life Sciences), employing the synthetic primers TA-AAAGCTTCACCACCACCACCACCA and AATTTTTGGAATTCCTGT-GAGTTC, which results in the loss of the sequence coding for the Gly-Ser-His$_6$ extension and the *Bam*H1 restriction site. The PCR parameters were 1 cycle of 5 s at 95 °C, 15 min at 50 °C, 4 min at 68 °C, followed by 14 cycles of 15 s at 95 °C, 30 s at 50 °C and 4 min at 68 °C, terminating with 20 min at 68 °C. The PCR products were purified with the Concert Rapid PCR purification system (Invitrogen), phosphorylated with phage T4 kinase (Promega), polished with DNA polymerase *Pwo* (Roche Applied Science), ligated with T4 DNA ligase (Promega), and the parental plasmid digested with *Dpn*I (Promega). *E. coli* DH5α cells were transformed with the ligated products, plasmid DNA was purified from individual transformants and employed to transform *E. coli* BL21(DE3) pLys for overexpression. The mutant plasmids were identified by the loss of the *Bam*H1 restriction site of the parental DNA and by sequencing their *ftsZ* gene, employing the sequencing primers *mf3* (ACCATATCTGAATCTTG), *mj1* (CGGCATATTTGGAAC), *p319y* (ATATATAATTGTAGCATTTGGGTCTAATCTTG) and *mj3* (GAA-CAATGGAGGCTTAGCG) with an Applied Biosystems PRISM 3700 DNA analyzer. The absence of the histidine tags in FtsZ and FtsZ-W319Y was confirmed by immunoblotting with anti-His antibody (Amersham Biosciences).

FtsZ and FtsZ-W319Y were overexpressed as described above for the His tag-containing proteins, but they were precipitated from the high speed supernatants of the cell lysates with 33% ammonium sulfate. The precipitate was resuspended in 50 mM Tris-HCl, 1 mM EDTA, 150 mM KCl, pH 8.0, clarified, and chromatographed in a HiTrap Q-HP anion exchange column (5 ml, Amersham Biosciences) with a gradient of 0.15–1.0 M KCl in the same buffer. FtsZ, which eluted at ~0.45 M KCl together with a ~98 kDa protein contaminant, was concentrated by ultrafiltration with Centriprep 30K (Amicon), and it was further purified by hydrophobic chromatography in a HiTrap Phenyl Sepharose HP column (1 ml, Amersham Biosciences) with a 0.8–0 M ammonium sulfate gradient in 50 mM potassium phosphate, 1 mM EDTA, pH 7.5. Purified FtsZ, which eluted at ~0.4 M ammonium sulfate, was concentrated, desalted with a Fast Desalting column (5-ml Sephadex G-25 superfine, Amersham Biosciences) equilibrated with 20 mM Tris-HCl, 1 mM NaN_3, 1 mM EDTA, pH 8.0, concentrated again, and stored at −80 °C). FtsZ-His$_6$ and FtsZ-W319Y-His$_6$ were purified as controls of this method and had the same assembly properties under standard conditions (described under "Results") as those purified by affinity chromatography. FtsZ from *E. coli* was purified and assembled as described (12, 21).

Purified FtsZ(wt), FtsZ-His$_6$, FtsZ-W319Y, and FtsZ-W319Y-His$_6$ were ≥90% homogeneous in an SDS-polyacrylamide gel. Their molecular masses, determined by MALDI-TOF mass spectrometry with an Applied Biosystems Voyager System 4242 instrument using yeast enolase as an external standard, were within experimental error of the theoretical values from the translated gene sequences. Their N-terminal ends were confirmed in each case by Edman microsequencing (results: Met-Lys-Phe-Leu) with an Applied Biosystems 477A sequencer equipped with on-line HPLC[1] analysis of the phenylthiohydantoin derivatives. Protein-bound guanine nucleotide was extracted, and protein and nucleotide concentrations were determined spectrophotometrically as described (21), employing for apo-FtsZ-W319-Y and apo-FtsZ-W319Y-His$_6$ the extinction coefficient value 2560 M^{-1} cm^{-1} at 280 nm in 6 M guanidinium chloride (calculated for 0 Trp, 2 Tyr, and 8 Phe residues). Purified FtsZ contained 0.4 ± 0.2 guanosine nucleotide bound (of which 73% was GTP and 27% GDP); FtsZ-His$_6$, 0.6 ± 0.1 (39% GTP, 61% GDP); FtsZ-W319Y, 0.5 ± 0.2 (98% GTP, 2% GDP); FtsZ-W319Y-His$_6$, 0.5 ± 0.1 (39% GTP, 61% GDP). The low GTP/GDP ratio of the affinity-purified His$_6$-tagged proteins was due to the purification method, since control FtsZ-His$_6$ and FtsZ-W319Y-His$_6$ purified by ammonium sulfate and ion exchange (see above) had 89% GTP-11% GDP and 95% GTP-5% GDP, respectively.

FtsZ(wt), FtsZ-His$_6$, FtsZ-W319Y, and FtsZ-W319Y-His$_6$ had practically identical far UV circular dichroism spectra. The guanidinium chloride unfolding curves of the four proteins could be fitted by two-state transition models, with identical half denaturant concentrations (average, 3.03 ± 0.10 M guanidinium chloride) and unfolding free energy changes (average, 11.6 ± 2.0 kcal mol^{-1}) within experimental error (for FtsZ-His$_6$, see Ref. 21). These results indicated that neither modification, the addition of the His$_6$ tag or the W319Y point mutation, had any detectable effects on the average secondary structure and on the stability of FtsZ to chemical unfolding.

Assembly, GTPase, and Bound Nucleotide Assays—FtsZ was diluted (≥20-fold) or chromatographically equilibrated into potassium-containing assembly buffer (50 mM Mes-KOH, 50 mM KCl, 1 mM EDTA, pH 6.5), or sodium-containing assembly buffer (50 mM Mes-NaOH, 50 mM NaCl, 1 mM EDTA, pH 6.5) at 30° (the FtsZ proteins with a six histidine tag had a tendency to precipitate in the cold), centrifuged for 10 min at 50,000 rpm in a Beckman TLA120.2 rotor to remove any aggregates, and its concentration was measured. Aliquots of FtsZ (typically 12.5 μM) were placed into a fluorometer cuvette thermostatted at 55 °C (solution temperatures were measured with a thermocouple), and its 350-nm light scattering was monitored at 90° (21). Assembly was typically started 5 min after by adding 6 mM $MgCl_2$ and 1 mM GTP (or 0.1 mM GMPCPP). Samples (20 μl) for electron microscopy were taken directly from the solution.

The GTP and GMPCPP hydrolyzing activities of FtsZ solutions maintained at 55 °C in a thermostatting block (Eppendorf Thermostat Plus) were measured by taking 20-μl samples at several times, extracting the nucleotide with cold 0.5 N $HClO_4$ (with guanosine as an internal standard), followed by neutralization and ionic pair HPLC analysis of nucleotides with an octadecyl silica column as described previously (25). The nucleotides bound to FtsZ polymers were analyzed by sedimentation (6 min at 60,000 rpm in a prewarmed Beckman TL100 rotor), followed by pellet resuspension, nucleotide analysis, and FtsZ concentration measurement.

Electron Microscopy and Image Processing—Samples were adsorbed to grids on a hot plate or mildly fixed with 0.5% glutaraldehyde and subsequently stained with 2% uranyl acetate. Images were taken at various magnifications with JEOL 1200EX-II microscopes operated at 100 kV, and recorded on Kodak SO-163 film. In the case of the FtsZ sheets, micrographs were recorded with a nominal magnification of ×40,000 and the 3 best images, as judged by optical diffraction, digitized in a Zeiss SCAI scanner with a sampling window corresponding to 3.5 Å/pixel. Lattice refinement of the images was carried out using the X-windows-based graphical environment SPECTRA (26) and the subsequent image processing, including lattice unbending, was performed using the MRC image processing suite (27). Transfer function correction was carried out using the Integrated Crystallographic Environment (ICE, Ref. 28). Images were merged with the program ORIGTILT (27), using for that the crystallographic group $p222_1$, which was suggested by the program ALLSPACE (29). In the case of the isolated filaments of FtsZ from *M. jannaschii* and from *E. coli*, images were taken at ×60,000 and digitized with a sampling window corresponding to 2.4 Å/pixel. 528 and 268 areas of the thick filaments were respectively selected so that 6 FtsZ monomers (3 of each of the 2 filaments) were present, and were subsequently aligned by cross-correlation free-pattern methods (30) and processed using the XMIPP software package (31).

RESULTS

Reversible Nucleotide-dependent Assembly of FtsZ from M. jannaschii—The polymerization of purified FtsZ was systematically investigated with light scattering at 90° and electron microscopy. Initial attempts to assemble FtsZ from *M. jannaschii* at moderate temperatures failed. However, increasing the temperature permitted the observation of reversible, GTP-Mg^{2+}-dependent archaeal FtsZ assembly, similarly to mesophilic bacterial FtsZs at lower temperatures. This is probably

[1] The abbreviations used are: HPLC, high performance liquid chromatography; GMPCPP, guanosine 5′-(α,β-methylenetriphosphate); Mes, 4-morpholineethanesulfonic acid.

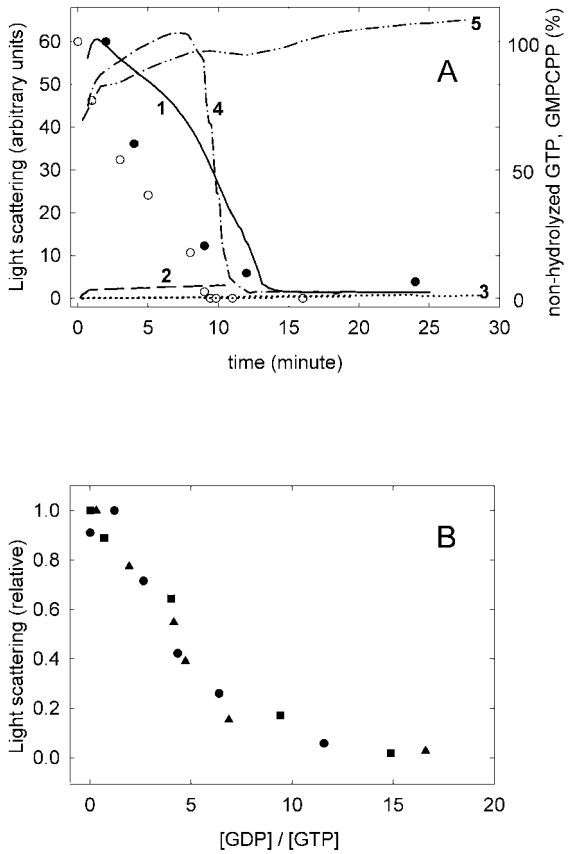

FIG. 1. *A*, assembly of FtsZ (12.5 μm) monitored by light scattering in potassium-containing Mes assembly buffer pH 6.5, at 55 °C. Assembly was started by addition of 6 mM $MgCl_2$ and nucleotide at time 0, as indicated below. *Trace 1*, assembly with Mg^{2+} and 1 mM GTP; *solid circles*, percent non-hydrolyzed GTP in the solution; *trace 2*, assembly with Mg^{2+} without added nucleotide; *trace 3*, results obtained with three different samples containing either Mg^{2+} and 2 mM GDP, or GDP, or GTP; *trace 4*, assembly with Mg^{2+} and 0.1 mM GMPCPP; *void circles*, percent GMPCPP in the same solution as trace 4; *trace 5*, assembly with Mg^{2+} and 1 mM GMPCPP. *B*, light scattering (relative to maximal) *versus* [GDP]/[GTP] ratio in FtsZ polymer solutions. The data were obtained from scattering and nucleotide measurements in experiments made as in *panel A*, started with 1 mM GTP and Mg^{2+}. *Circles*, with 3 mM Mg^{2+}; *squares*, 6 mM Mg^{2+}; *triangles*, 10 mM Mg^{2+}.

related to the fact that this hyperthermophilic archaeon has an optimal growth temperature of 85 °C (32). Fig. 1*A* (*trace 1*) shows the time course of assembly of FtsZ (wt, 12.5 μM) initiated by addition of 1 mM GTP and 6 mM $MgCl_2$ in potassium-containing Mes assembly buffer, pH 6.5, at 55 °C, which were chosen as standard conditions. Prior to nucleotide addition at time zero, the light scattering was negligible. Twenty seconds later (the shortest time recorded) most of the large scattering increase due to FtsZ assembly had taken place, and it gradually decayed afterward following the hydrolysis of GTP to GDP (the *solid circles* in Fig. 1*A* are HPLC measurements of the GTP concentration in the solution). Addition of more GTP produced a new cycle of assembly and disassembly; the FtsZ polymers completely disassembled upon GDP addition in less than 20 s. Polymers could be also cycled by cooling and heating the solution, or by chelation of Mg^{2+} with EDTA followed by excess Mg^{2+} addition (not shown). A very small light scattering increase was observed with Mg^{2+} only, and an insignificant increase with GDP and Mg^{2+}, or with GTP or GDP only (Fig. 1*A*), indicating that similarly large polymers did not assemble under these conditions. Substitution of GTP by the slowly hydrolyzable analogue GMPCPP permitted prolonged assembly (Fig. 1*A*) during ≥2 h. Decreasing the GMPCPP concentration to 0.1 mM resulted in a shorter assembly, which dropped following hydrolysis of the analogue (Fig. 1*A*).

TABLE I
GTPase and GMPCPPase activities of FtsZ from M. jannaschii

Protein	Conditions[a]	GTP hydrolysis rate
		min^{-1}
FtsZ (wt)	K^+	5.9 ± 0.6
	K^+, no Mg^{2+}	0.02 ± 0.01
	Na^+	0.01 ± 0.01
≤ 1 μM FtsZ(wt)	K^+	0.26 ± 0.07
FtsZ-His_6	K^+	6.0 ± 0.5
	Na^+	0.04 ± 0.01
≤ 1 μM FtsZ-His_6	K^+	0.11 ± 0.06
FtsZ-W319Y-His_6	K^+	0.02 ± 0.01
FtsZ-W319Y	K^+	0.07 ± 0.02
Protein	**Conditions[b]**	**GMPCPP hydrolysis rate**
		min^{-1}
FtsZ (wt)	K^+	0.71 ± 0.04
	Na^+	0.00 ± 0.01
FtsZ-His_6	K^+	0.50 ± 0.24
	Na^+	0.04 ± 0.02

[a] Measurements were made by HPLC from 12 μM FtsZ solutions incubated with 1 mM GTP in 50 mM Mes-KOH, 50 mM KCl, 1 mM EDTA, 6 mM $MgCl_2$, pH 6.5 at 55 °C, unless otherwise indicated (a minimum of two independent determinations were made per measurement). Conditions listed are: K^+, this potassium-containing buffer; Na^+, same buffer made with NaOH and NaCl.

[b] Measurements of GMPCPP hydrolysis were made with 0.1 mM GMPCPP; the hydrolysis rate by FtsZ (wt) did not increase with 1 mM GMPCPP.

Polymerizing FtsZ hydrolyzed one GTP per ~10 s at pH 6.5 and 55 °C (Table I). Increasing the Mg^{2+}concentration decreased the rate of GTP hydrolysis and increased the time stability of the FtsZ polymers. Half disassembly (50% of the maximal scattering value) was reached in ~4 min with 3 mM $MgCl_2$, whereas it typically took about 9 min with 6 mM $MgCl_2$ and 12 min with 10 mM. Interestingly, disassembly of FtsZ closely followed the consumption of GTP in each of these cases. Fig. 1*B* shows a plot of the light scattering *versus* the GDP/GTP ratio of the solution, measured in these experiments. The relative light scattering intensities (which started from different absolute values at each $MgCl_2$ concentration) drop practically together upon hydrolysis of GTP. Similar observations were made with FtsZ-His_6, with the difference that the polymers were apparently stable for ≥60 min with 10 mM $MgCl_2$.

After sedimentation (a total of ~8 min at 55 °C) the FtsZ polymers were found to contain a large proportion of hydrolyzed nucleotide. Pellets from FtsZ polymers assembled in K^+-containing buffer with 5 mM GTP and 10 mM $MgCl_2$ contained 67% GTP and 33% GDP (supernatant: 89% GTP, 11% GDP). With 1 mM GMPCPP and 6 mM $MgCl_2$ they contained 53% GMPCPP and 47% GMPCP (supernatant: 94% GMPCPP, 6% GMPCP).

FtsZ with GTP and Mg^{2+} mainly formed filamentous polymers of widths usually between 120 and 300 Å (see Fig. 2*A*). FtsZ with GMPCPP and Mg^{2+} formed polymers (Fig. 2*C*) as well that were typically wider (~800 Å) than the GTP-induced polymers. Together with the large GTP and GMPCPP polymers, isolated ~60 Å wide FtsZ filaments, straight (Fig. 2*A*) and curved (Fig. 2*B*), could be also observed. FtsZ at 80 °C, close to the 85 °C optimal growth temperature of *M. jannaschii* (32), assembled with GTP and Mg^{2+} similarly at 55 °C.

FtsZ-His_6, which is FtsZ with a C-terminal Gly-Ser-His_6 extension, initially employed for purification and crystallization (19, 24), assembled similarly to FtsZ under our standard conditions at 55 °C (not shown). However, upon modification of these conditions, FtsZ-His_6 showed significant differences with FtsZ. These included (i) the assembly into helical tubes (Fig.

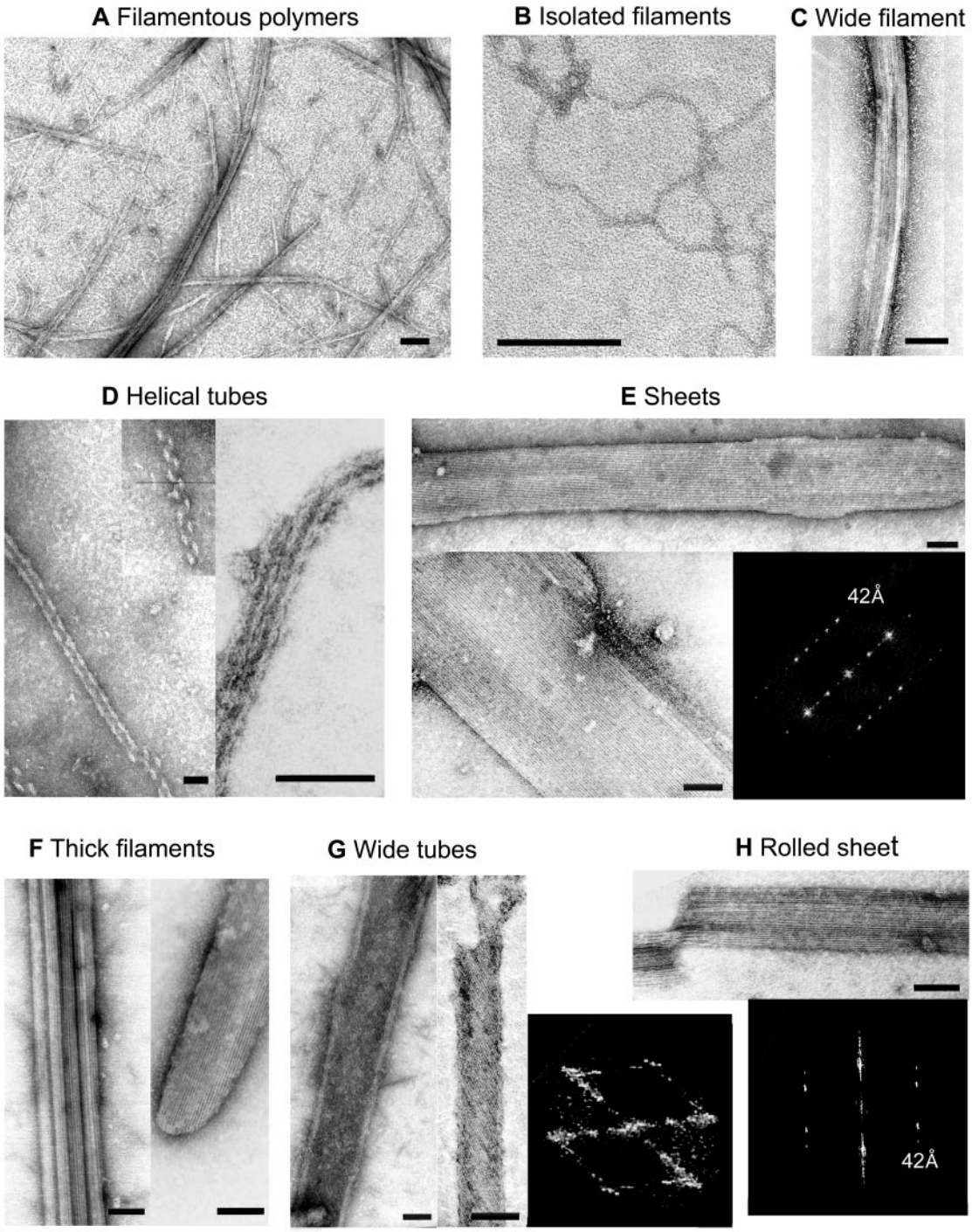

FIG. 2. **Representative electron microscopy images of each type of FtsZ polymer observed in this work.** The diffractograms shown in *E*, *G*, and *H* are beside their corresponding micrographs. The conditions for the assembly of these polymers are listed in Table II and are described in the text. The *bars* correspond to 1000 Å.

2*D*) with Ca^{2+} (instead of Mg^{2+}) and also with Na^{+} (instead of K^{+}), (ii) polymerization with Na^{+} without added nucleotide forming wide tubes (Fig. 2*G*), and (iii) formation of ordered sheets (Fig. 2*E*) upon assembly at 80 °C with Mg^{2+} (with GTP, GDP, or without added nucleotide). The above results indicated that the γ phosphate of the guanosine nucleotide and Mg^{2+} promote FtsZ assembly; they suggested that nucleotide hydrolysis by the polymer results in its disassembly, and that the six histidine extension enhances assembly, favoring the formation of helical and laminar polymers instead of the filamentous polymers. The structures of the different polymers and of the FtsZ filaments will be addressed later.

Activation of FtsZ GTPase by Assembly in K^{+}-containing Buffer—GTP-induced assembly of FtsZ into large light scattering polymers and significant GTP hydrolysis were found to take place above a critical FtsZ concentration (Cr $\simeq$ 2 μM FtsZ). FtsZ assembly measured by sedimentation is cooperative and proceeds above a critical protein concentration in a nucleated condensation polymerization reaction.[2] Fig. 3 shows parallel measurements of GTP hydrolysis and light scattering at varying FtsZ concentration, indicating that the unassembled FtsZ

[2] S. Huecas and J. M. Andreu, submitted for publication.

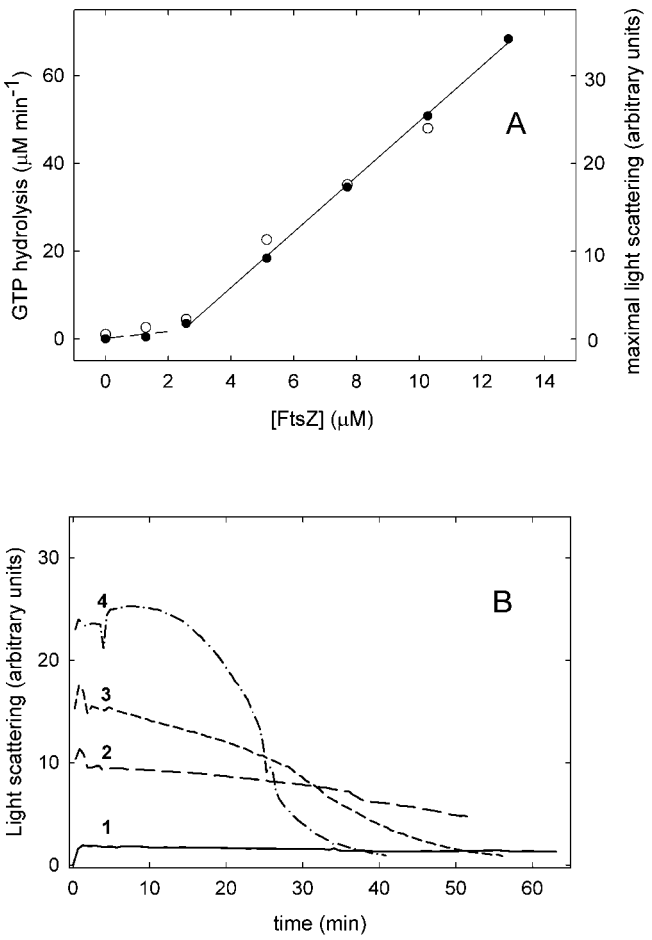

FIG. 3. *A*, critical concentration plots of FtsZ GTPase and assembly in potassium-containing Mes assembly buffer pH 6.5, at 55 °C. *Solid circles* (left ordinate scale), GTPase activity; *void circles* (right ordinate scale), light scattering. Note that light scattering is not necessarily proportional to polymer concentration (46). *B*, time course of assembly at several concentrations of FtsZ. *Trace 1*, 2.6 μM; *trace 2*, 5.1 μM; *trace 3*, 7.7 μM; *trace 4*, 10.3 μM.

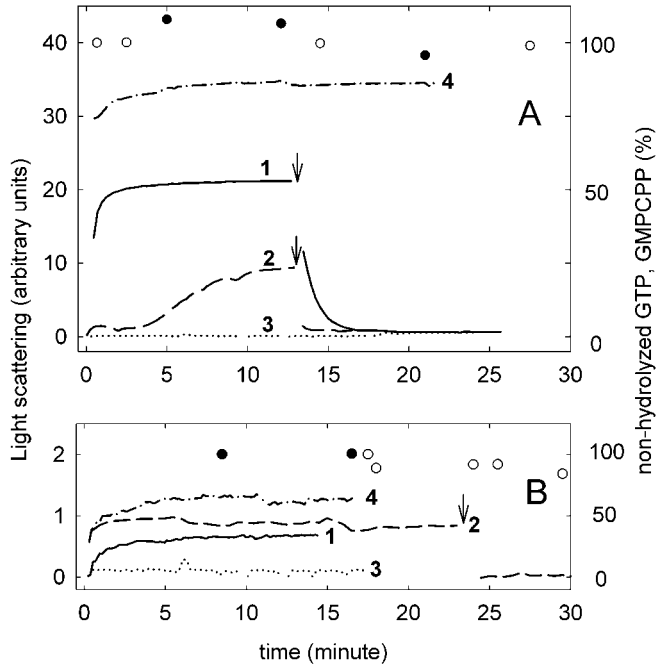

FIG. 4. *Panel A*, assembly of FtsZ-His6 (12.5 μm) monitored by light scattering in sodium-containing Mes assembly buffer pH 6.5, at 55 °C. Assembly was started by addition of 6 mM $MgCl_2$ and nucleotide as indicated. *Trace 1*, assembly with Mg^{2+} and 0.1 mM GTP; *solid circles*, percent non-hydrolyzed GTP in the solution; *trace 2*, with Mg^{2+} without added nucleotide; *trace 3*, results obtained with different samples containing either Mg^{2+} and 2 mM GDP, or GDP, or GTP; *trace 4*, with Mg^{2+} and 0.1 mM GMPCPP; *void circles*, percent GMPCPP in the same solution. At the points indicated by *arrows*, 2 mM GDP was added to the corresponding solutions. *Panel B*, results obtained with untagged wild-type FtsZ. Symbols are as in *panel A*.

below Cr hydrolyzed ~0.3 GTP per minute, whereas assembled FtsZ hydrolyzed 6.2 GTP per minute. Similar observations were made with FtsZ-His_6.

Nucleotide hydrolysis could be uncoupled from the assembly of FtsZ by replacing K^+ by Na^+ in the buffer, or with a point mutation inactivating the GTPase activity. Fig. 4 shows the time courses of assembly and nucleotide consumption in sodium-containing Mes assembly buffer at 55 °C. The nucleotide hydrolysis rate decreased more than 100-fold with respect to the rate with K^+ (Table I). Under these conditions FtsZ-His_6 (12.5 μM) formed stable helical tubes (Fig. 2*D*) with GTP or GMPCPP plus Mg^{2+}, and also with Mg^{2+} only, but not with GDP plus Mg^{2+} (since GDP is inhibitory, the polymer induction by Mg^{2+} alone may be attributed to the residual GTP in purified FtsZ; see "Experimental Procedures"). The FtsZ-His_6 polymers assembled with GTP were found to contain 94% GTP and 6% GDP. Interestingly, addition of excess GDP to these non-hydrolyzing FtsZ-His_6 polymers in Na^+ buffer resulted in their rapid disassembly (half-disassembly time, 40 s; Fig. 4*B*). FtsZ in Na^+ buffer assembled into weakly light scattering stable polymers, which did not hydrolyze nucleotide but disassembled by GDP addition in ≤30 s (Fig. 4*B*).

Assembly of the GTPase-inactive Mutant FtsZ-W319Y-His_6—FtsZ and FtsZ-His_6 assemble in a GTP and Mg^{2+}-dependent fashion, forming polymers that can hydrolyze GTP, as shown above. The mutation of FtsZ-His_6 into FtsZ-W319Y-His_6, was chosen to be investigated due to the location of the single tryptophan (Trp-319) at the GTPase-activating interface of FtsZ, and the low natural frequency of the Trp → Tyr substitution at this position. This mutation inhibits the GTPase activity of FtsZ polymers and it favors the formation of stable ordered assemblies. Fig. 5 shows the time course of assembly of FtsZ-W319Y-His_6. Assembly was induced by GTP plus Mg^{2+}, and by Mg^{2+} alone, but not by GDP and Mg^{2+}. This is qualitatively similar to the results of inhibiting the GTPase by Na^+/K^+ substitution (Fig. 4), except that GDP addition failed to reproducibly induce disassembly. The GTPase activity was similarly reduced, at least by two orders of magnitude (Table I). The Mg^{2+}-induced assembly without added nucleotide (Fig. 5) may be explained by the residual GTP bound to purified FtsZ-W319Y-His_6. The main structures formed by FtsZ-W319Y-His_6 where large ordered two-dimensional polymers made of filaments (Fig. 2*E*). Other structures formed by FtsZ-W319Y-His_6, at 80 °C, were rolled sheet polymers (Fig. 2*H*) in K^+-containing buffer without nucleotide or Mg^{2+}, and also thick filamentous polymers formed with Mg^{2+} plus GTP or GDP (Fig. 2*F*). Assembly of FtsZ-W319Y has only been observed at 80 °C, forming thick polymers (Fig. 2*F*), indicating that the polymerization of FtsZ-W319Y-His_6 is facilitated by the six histidine extension. FtsZ-W319Y-His_6 coassembled with FtsZ-His_6. A double mutant FtsZ-W319Y-T92W-His_6 (23) assembled poorly under these conditions; however it also coassembled with FtsZ-His_6, stabilizing it against disassembly by GTP consumption, and forming similar laminar structures (Fig. 2*E*).

The Polymorphic Assembly Products of Purified FtsZ—The assembly products of purified FtsZ were different types of polymers, depending on the solution conditions, as indicated by Table II. Representative electron micrographs of each polymer

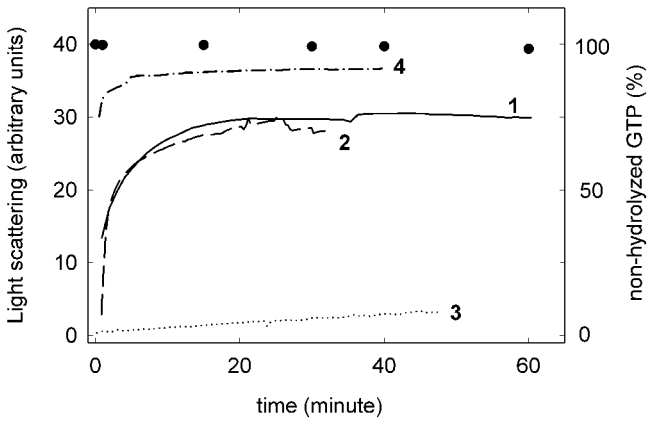

FIG. 5. **Assembly of mutant FtsZ-W319Y-His$_6$ (12.5 μm) monitored by light scattering in potassium-containing Mes assembly buffer pH 6.5, at 55 °C.** *Trace 1*, assembly with Mg^{2+} and 1 mM GTP; *solid circles*, percent non-hydrolyzed GTP in the solution; *trace 2*, with Mg^{2+} without added nucleotide; *trace 3*, results obtained with different samples containing either Mg^{2+} and 2 mM GDP, or GDP, or GTP; *trace 4*, with Mg^{2+} and 0.1 mM GMPCPP.

type are shown in Fig. 2. For a short summary, FtsZ and FtsZ-His$_6$ under standard GTP-Mg^{2+}-K^+ assembly conditions formed filamentous polymers and isolated straight filaments (Fig. 2*A*), isolated curved filaments (Fig. 2*B*), and they also formed wide filamentous polymers with GMPCPP (Fig. 2*C*). FtsZ-His$_6$ assembled into helical tubes (Fig. 2*D*) with Ca^{2+} and also formed wide tubes with Na^+ (Fig. 2*G*). The inactivated GTPase mutant FtsZ-W319Y-His$_6$ assembled into sheet polymers (Fig. 2*E*) and helical tubes (Fig. 2*D*) under standard conditions. Each of these polymers was observed in good yield and assembled in a reversible, biochemically regulated manner, including induction by nucleotide triphosphate and Mg^{2+} at 55 °C, and inhibition by GDP.

The images of sheets (Fig. 2*E*) gave similar diffraction patterns showing a tubulin-like axial spacing between FtsZ subunits in a unit cell of dimensions ~42 Å to ~140 Å (Fig. 2*E*). These sheets were readily obtained from FtsZ-W319Y-His$_6$. Their structural features are very similar to those of the minoritary Ca^{2+} two-dimensional crystals and the GMPCPP sheets studied by Löwe and Amos (5, 33). The helical tubes of FtsZ-His$_6$ have a diameter of ~320 Å and unwind in some segments revealing their helicity (Fig. 2*D*). Wide tubes (Fig. 2*H*) form under related conditions (Table II). The helical tubes appear closely related to the hollow helical tubes formed with Ca^{2+} and GMPCPP (5, 33). The isolated filaments are roughly 60 Å wide (Fig. 2*B*), and appear to be similar to the filaments typically formed by assembly of bacterial FtsZ from *E. coli* (12, 21). We could not obtain diffraction patterns of the filamentous polymers (Fig. 2*A*).

These results suggest that the different polymers may involve basically similar FtsZ filaments, with variations in the lateral filament interactions leading to the assembly of the filamentous, helical, sheet, or tube polymers. The fact that the wild-type FtsZ formed filamentous polymers instead of the large well-ordered sheet and helical tube polymers formed by FtsZ-His$_6$ and FtsZ-W319Y-His$_6$, suggest that the two-dimensional crystallization is facilitated by the six histidine extension, which possibly makes interactions inducing the ordered lateral association of the FtsZ-His$_6$ filaments, whereas FtsZ(wt) filaments laterally associate in a more disordered fashion. Therefore it appears that the FtsZ-His$_6$ sheet and tubes contain additional features not present in the more natural polymers of FtsZ(wt). However, they proved useful to investigate the FtsZ filament structure.

FtsZ Double-stranded Filament Structure—The analysis of the images of selected single-layered ordered sheets generated by FtsZ-W319Y-His$_6$ (Fig. 6, *A* and *B*) revealed similar features to those described by Löwe and Amos (5) for the FtsZ-His$_6$ Ca^{2+}-induced sheets, a series of filaments running along the sheet axis. The three-dimensional reconstruction carried out by these authors on the FtsZ-His$_6$ Ca^{2+}-induced sheets showed that the filaments are formed by two parallel FtsZ protofilaments and that the thicker filaments interact with each other in an antiparallel fashion. The processing and merging of some of the ordered sheets obtained by us (Fig. 6*A*) suggested an identical arrangement (Fig. 6*C*). Comparison of phases of symmetry-related reflections (29) pointed, as in the case of the FtsZ-His$_6$ Ca^{2+}-induced sheets, to $p222_1$ as the proper crystallographic group, and the images were combined accordingly. The projection map revealed the same antiparallel arrangement of thick filaments formed by two parallel protofilaments, with thin connections between neighbor thick filaments (*arrow* in Fig. 6*C*). Interestingly, when polymers of wild-type FtsZ were visualized at the electron microscope, a reasonable percentage of thick filaments, either individually or forming part of disordered sheets could be observed (Fig. 6*D*). The averaging of several hundred small areas of individual filaments generated an image (Fig. 6*E*), which reveals more clearly the double protofilament nature of the thick filaments, with the FtsZ monomers of each protofilament running in parallel. The polar appearance of the thick filament in the mutant FtsZ sheets is lost by the averaging procedure and the lack of visible connections in the wild-type FtsZ filaments. Whereas the longitudinal repeating distance of the protofilament in the crystal structure (Fig. 6*C*) and in isolated filaments (Fig. 6*E*) is almost identical (43 and 44 Å, respectively), there is an apparent discrepancy with respect to the width of the thick filament in both types of structures (57 *versus* 88 Å). However, this can be explained by the fact that the thick filament represented in Fig. 6*C*, according to the three-dimensional reconstruction of the FtsZ-His$_6$ Ca^{2+}-induced sheets carried out by Löwe and Amos, is tilted (see Fig. 3*B* of Ref. 5) and therefore its projection is smaller.

Finally, when the filaments formed by bacterial FtsZ from *E. coli* under our experimental conditions (Fig. 6*F*) were subjected to the same averaging procedure, an almost identical double-stranded filament image was obtained (Fig. 6*G*).

DISCUSSION

Dynamic Assembly of FtsZ from M. janaschii Is Induced by GTP and Mg^{2+} at High Temperature, and It Activates GTP Hydrolysis Leading to Polymer Disassembly—This work first established the conditions for reversible biochemically regulated assembly of archaeal FtsZ from *M. jannaschii*, and indicated that FtsZ is activated by GTP binding for Mg^{2+}-induced assembly. Assembled FtsZ(wt) hydrolyzes one GTP every ~10 s (depending on conditions), and when GDP becomes predominant in the solution the polymers disassemble. This provides the more basic features for archaeal FtsZ polymer assembly/disassembly dynamics, similarly to bacterial FtsZ (9). In addition to the known dependence of GTPase activity of bacterial FtsZ on protein concentration (15, 34, 35), our results with archaeal FtsZ most clearly indicate that the enhancement of the GTPase activity is cooperatively induced by the intermolecular contacts between the FtsZ molecules in large polymers, which were detected in the same experiment above a critical concentration of FtsZ (Fig. 3). The low GTPase values of unassembled FtsZ might be attributed to contacts in FtsZ oligomers (35) or to a basal activity of FtsZ monomers. Adding a C-terminal His$_6$ tag to FtsZ had little effect on its GTPase or assembly (monitored by light scattering and electron microscopy) under our standard conditions. However, it was shown to enhance assembly under other conditions, allowing polymeri-

TABLE II
Polymer structures assembled from purified M. jannaschii FtsZ

Protein	Conditions[a]	Polymer structures observed[b]
FtsZ (wt)	Standard	Filamentous polymers (A), isolated filaments (B)
	GMPCPP	Wide filaments (C), filamentous (A), filaments (B)
	GMPCPP, Na^+	Isolated filaments (B)
	Ca^{2+}	Filamentous polymers (A)
FtsZ-His_6	Standard	Filamentous polymers (A), filaments (B)
	Na^+	Helical tubes (D), filamentous polymers (A)
	Na^+, no GTP	Wide tubes (G)
	GMPCPP	Wide filaments (C), filaments (B)
	GMPCPP, Na^+	Helical tubes (D), filamentous polymers (A)
	Ca^{2+}	Helical tubes (D)
	80 °C (GTP, GDP or no nucleotide)	Sheet (E)
	80 °C, no Mg^{2+}	Filamentous polymers (A)
FtsZ-W319Y-His_6	Standard	Sheet (E), helical tubes (D)
	No GTP	Sheet (E)
	GMPCPP	Helical tubes (D), sheet (E)
	80 °C (GTP or GDP)	Thick filaments (F)
	80 °C, no nucl, no Mg^{2+}	Rolled sheet (H)
FtsZ-W319Y	80 °C (GTP, GDP or GMPCPP)	Thick filamentous (F)

[a] Standard assembly conditions were 12 μM FtsZ in 50 mM Mes-KOH, 50 mM KCl, 1 mM EDTA, 6 mM $MgCl_2$, 1 mM GTP, pH 6.5 at 55 °C. Only the modifications or substitutions giving significatively different polymers are listed. Na^+ indicates buffer made with sodium instead of potassium; Ca^{2+}, calcium instead of magnesium. GMPCPP was 0.1 mM (FtsZ(wt) with 1 mM GMPCPP gave the same morphology), GDP was 2 mM, $CaCl_2$ was 6 mM (instead of $MgCl_2$).

[b] Each polymer type is identified with a letter in parenthesis (A, B, etc.) corresponding with the representative electron micrographs shown in each panel of Fig. 2.

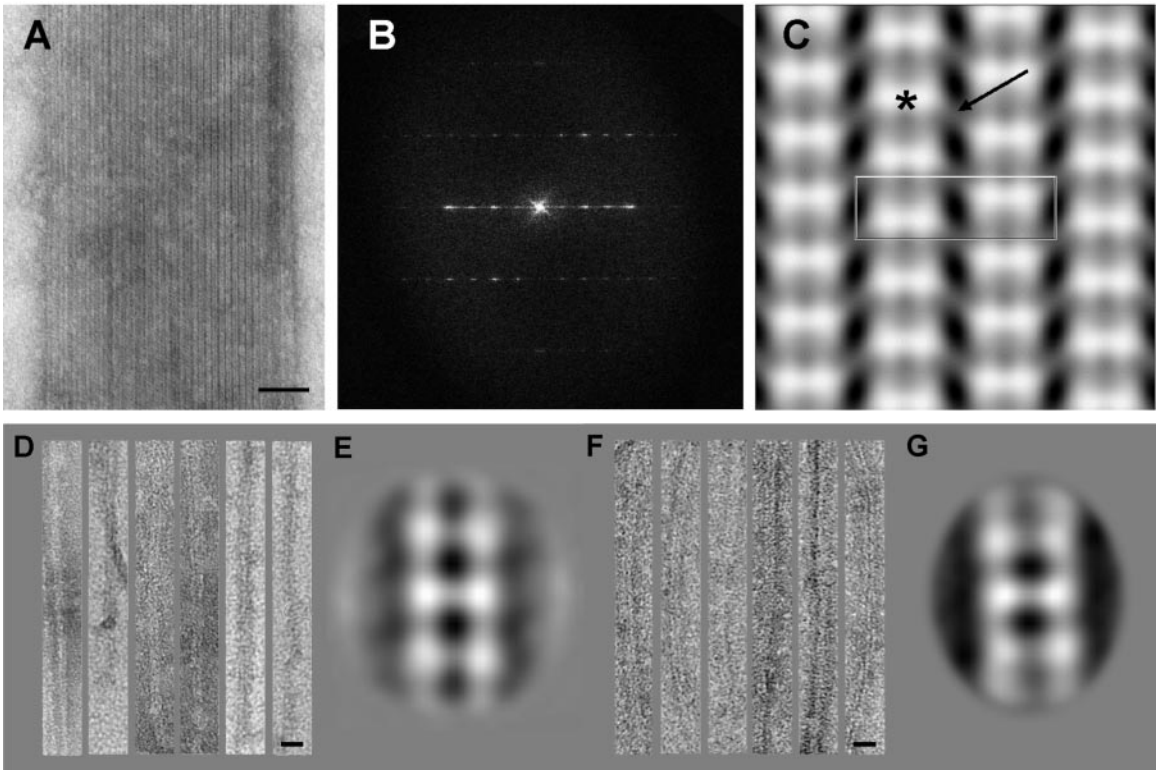

FIG. 6. **Image processing of ordered sheets of FtsZ-W319Y-His_6 from *M. jannaschii*, and of thick filaments of wild-type FtsZ from *M. jannaschii* and from *E. coli*.** *A* shows a micrograph of an ordered array of FtsZ-W319Y-His_6 whereas *B* shows its computed diffraction pattern and *C* a projection map generated using $p222_1$ symmetry. The rectangle in *C* indicates the unit cell of the crystal, which contains four FtsZ monomers, whereas the *asterisk* and the *arrow* indicate respectively to the connection between monomers belonging to the same thick filament or to an opposing one. *D* shows a gallery of individual thick filaments and *E* the average image obtained after processing 528 areas extracted from individual thick filaments. *F* shows a similar gallery of the products of assembly of bacterial FtsZ from *E. coli* (20 μM FtsZ in 50 mM Mes-KOH, 50 mM KCl, 2 mM dithiothreitol, 10 mM $MgCl_2$, and 1 mM GTP, pH 6.5, 30 °C) and *G* the average image obtained from 268 areas from these filaments. The bar in *A* represents 1000 Å, and the bars in *E* and *F* 100 Å.

zation by Ca^{2+} addition without added GTP, or in Na^+-containing buffer, or at 80 °C, with the formation of helical tubes, ordered sheet, and tubes, instead of filamentous polymers (see "Results," Table II, and Fig. 5).

Currently available results do not clarify the mechanism of FtsZ polymer dynamics, that is, whether the hydrolyzed nucleotide exchange takes place in the FtsZ polymers or in rapidly assembling and disassembling FtsZ monomers. In the first case (nucleotide site exchangeable in the polymer; Ref. 14), the FtsZ polymers would tend to be continuously assembled in the GTP-containing cytosol, and FtsZ polymer destabilizing proteins would be absolutely required for regulation of the Z-ring. In the second case (nucleotide site occluded by assembly; a GDP polymer possibly stabilized by a GTP cap, as in tubulin; Ref. 14)

individual polymers would be intrinsically unstable once their subunits have hydrolyzed GTP, and stabilizing factors would be required. Our finding of a mixture of GTP and GDP in the sedimented polymers of *M. jannaschii* FtsZ would argue against immediate GTP hydrolysis and a GDP-polymer model (17); if confirmed with a faster separation method, it would also argue against a GTP-polymer model (16), and would favor the possibility that FtsZ forms mixed polymers whose stability is related to the proportion of GTP-bound and GDP-bound subunits.

FtsZ Assembles without GTP Hydrolysis in Na^+-containing Buffer and Disassembles by GDP Addition—The results of replacing K^+ by Na^+ in the assembly buffer conclusively showed that GTP or GMPCPP hydrolysis is not necessary for FtsZ assembly. They also indicated that the six histidine extension in FtsZ-His_6 induces helical assembly, which is not observed with wild-type archaeal FtsZ. The GTPase activities of bacterial FtsZ from *E. coli* (36) and from the archaeon *Haloferax volcanii* (37) have a similar K^+ cation requirement, whereas FtsZ from *Azotobacter vinelandii* and from *Thermotoga maritima* were reported equally active with Na^+ and K^+ (11) (in contrast with tubulin, which upon microtubule assembly hydrolyzes GMPCPP faster with Na^+ than with K^+; Ref. 38). These and other reports (8–10, 15, 16, 20) showed the modulation of FtsZ assembly and GTPase by monovalent and divalent cations; however, when FtsZ assembly took place it entailed significant nucleotide hydrolysis. Our results with *M. jannaschii* FtsZ in Na^+-containing assembly buffer provide for the first time non-hydrolyzing polymers of wild-type FtsZ. Interestingly, when GDP is added to mimic GTP hydrolysis these kinetically stabilized archaeal FtsZ polymers rapidly disassemble (Fig. 4). This confirms the role of GDP in FtsZ disassembly dynamics, and intuitively favors the notion of an exchangeable nucleotide binding site in these polymers, which would not be expected to exchange their subunits in such a short time, or alternately, a very rapid endwise disassembly.

The W319Y Mutation Inactivates the GTPase and Kinetically Stabilizes the FtsZ Polymers—A number of mutations have been shown to inhibit the GTPase activity of bacterial FtsZ, including the temperature sensitive *E. coli* mutant *ftsZ84* (39). Of special interest are the mutants in the longitudinal contact interface between FtsZ monomers, including the mutants at conserved loop T7, which has been proposed to come in close contact with the GTP bound to the next monomer down the filament (4, 5). Aspartate 212 is an essential residue for the GTPase activity of *E. coli* FtsZ (40–42). The corresponding residue Asp-238 (or one of the close residues Asn-233 or Asp-235) is thought to activate GTPase hydrolysis in *M. jannaschii* FtsZ, similarly to the putative activation of β-tubulin GTPase by residue Glu-254 of α-tubulin (4, 5). The single tryptophan residue Trp-319 of FtsZ from *M. jannaschii* is located at the bottom association interface of FtsZ, less than 10 Å away from co-catalytic loop T7. The new mutant FtsZ-W319Y-His_6 assembled without hydrolyzing GTP. From 64 FtsZ sequences aligned from the SwissProt data base, the residues at the position corresponding to Trp-319 of *M. jannaschii* FtsZ were mainly Phe (25) and Trp (15), followed by Leu (6), Val (5), Ala (4), Ile (3, including Ile-294 of *E. coli* FtsZ), and less frequently Arg (2), His (1), or Tyr (Ref. 1; *Borrelia burgdofei* FtsZ), suggesting that an adventitious interaction of the Tyr hydroxyl group, or its reduced hydrophobicity, are not well tolerated by the functionality of FtsZ. Note that FtsZ-W319Y assembled poorly with respect to FtsZ, indicating that the mutation also affects *in vitro* FtsZ assembly, which is probably rescued by the His_6 tag in FtsZ-W319Y-His_6.

The Basic Archaeal FtsZ Polymer Structure Is a Pair of Symmetric Tubulin-like Protofilaments—FtsZ, FtsZ-His_6, and FtsZW319Y-His_6 assembled into polymorphic filamentous structures, suggesting a common type of filament with different lateral associations. Our results, obtained under biochemically regulated assembly conditions, confirm the basic double-stranded structure of FtsZ-His_6 filaments induced by Ca^{2+} (5). The manual docking of the atomic structure of FtsZ from *M. jannaschii* into the three-dimensional reconstruction of the FtsZ protofilaments carried out by Löwe and Amos (5) suggests an arrangement of the FtsZ monomers within the protofilament similar to that of tubulin protofilaments. According to these authors, β-strand S3 is responsible of the interaction between protofilaments that form the thick filament (*asterisk* in Fig. 6*C*) whereas the C-terminal region (which is disordered in the x-ray crystal structure, and has an extra 8-residues fragment, including a six histidine tag) could bridge neighbor thick filaments (*arrow* in Fig. 6*C*). Since this extra region is not present in naturally occurring FtsZ, which generates laterally unordered filamentous polymers instead of ordered sheets, it is reasonable to suggest that these sheets are artificial and generated by the presence of the extra C-terminal residues. On the other hand it is likely that the interaction between two protofilaments is natural and gives rise to the thick filaments. This is confirmed by the novel image analysis of the filaments of wild-type FtsZ from *M. jannaschii* and also from *E. coli* (Fig. 6, *E* and *G*), which indicate that many of them are similarly made of two parallel protofilaments with the same axial spacing between monomers. Whereas *in vitro* FtsZ polymers were reported to be made of one (15), two, or several protofilaments (9, 12, 16, 20, 21), image processing (Fig. 6) defines the double-stranded filament as a basic unit of FtsZ assembly.

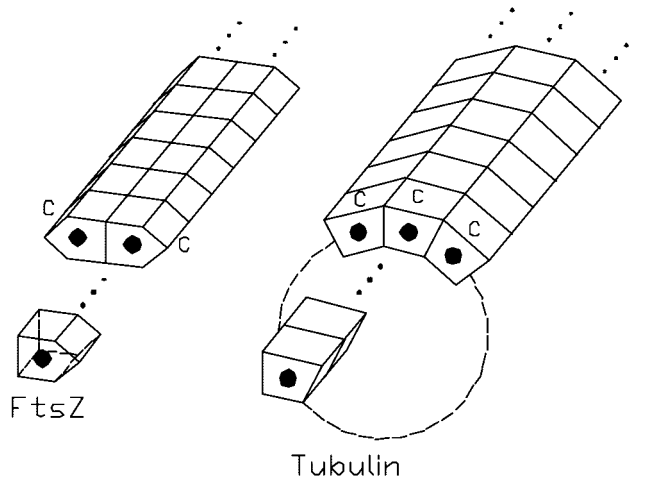

FIG. 7. **A simplified geometrical comparison of the mode of assembly of FtsZ proposed in this work with the known assembly of tubulin.** The *filled circles* indicate the position of the nucleotide and the *letter C* that of the C-terminal ends. FtsZ monomers assemble into a pair of symmetric protofilaments. Tubulin dimers assemble into similar protofilaments, which associate side to side by means of different interactions, until cylindrically closing into a microtubule.

The lateral interactions between two symmetric protofilaments of archaeal FtsZ are clearly different from those between microtubule protofilaments, as schematically depicted in Fig. 7. In this new assembly model the two FtsZ protofilaments cannot use their common lateral bonding interface to further associate, whereas the same lateral interactions between tubulin protofilaments are known to propagate indefinitely until reaching cylindrical closure (43). In addition, neighbor microtubule protofilaments are staggered by 9D, whereas the symmetrical FtsZ protofilaments are not. The lateral association interfaces of tubulin map to its characteristic loop insertions that are absent from FtsZ, and which we have proposed to have evolved

with extended two-dimensional polymerization (21), a feature which has not been observed in spontaneous *in vitro* assembly of natural FtsZ. The common fold of tubulin and FtsZ is thus employed to construct apparently similar protofilaments, however, these protofilaments further associate to perform different functions. The microtubules of the eukaryotic mitotic spindle are numerous large stiff polymers, roughly perpendicular to the cell division plane, which push and pull chromosomes for DNA segregation. The Z-ring marks the cell division plane for prokaryotic cytokinesis and directs the formation of the septum, but has not been actually shown to perform any mechanical constriction work. It may be speculated that these different functions have evolved from a common ancestor, by means of two different modes of protofilament accretion, the robust tubular assembly of tubulin and a simple protofilament pair in the case of FtsZ.

It is possible that FtsZ polymers in bacteria share the double-stranded filament structure, and that the Z-ring may be made of a few double stranded filaments, which have resisted observation by electron microscopy. In the prokaryotic cytosol, FtsZ polymerization and lateral association of the FtsZ polymers is specifically modulated by interaction with the other cell division proteins (2, 3). It can be calculated (8, 18) from an estimate of the average number of FtsZ molecules per *E. coli* and the cell diameter (11), and the 43 Å axial spacing between FtsZ monomers (see "Results"), if only a part (~30%) of FtsZ was incorporated into the Z-ring (6), that there might be as little as 3.5 continuous turns (on average) of FtsZ filament in a dividing cell. A similar calculation for *B. subtilis* cells (44) gives just a single functional FtsZ protofilament pair per Z-ring. Alternately, the Z-ring might be a scaffold made of $\geq$ 10 FtsZ double-stranded filaments (similar to the wider filament in Fig. 5*C*), whose *in vitro* formation is favored by macromolecular crowding[2] (45), but more FtsZ molecules would be needed to form such a ribbon-like Z-ring.

Acknowledgments—We thank Drs. J. Mingorance (CNB, CSIC, Madrid) and J. F. Díaz (CIB, CSIC, Madrid) for helpful discussions, Martín Alba (CIB, CSIC, Madrid) for technical assistance, and Dr. David Andreu (Universitat Pompeu Fabra, Barcelona) for mass spectrometry.

REFERENCES

1. Lutkenhaus, J. (2002) *Curr. Opin. Microbiol.* **5,** 548–552
2. Buddelmeijer, N., and Beckwith, J. (2002) *Curr. Opin. Microbiol.* **5,** 553–557
3. Margolin, W. (2003) *Curr. Biol.* **13,** 16–18
4. Nogales, E., Downing, K. H., Amos, L. A., and Löwe, J. (1998) *Nat. Struct. Biol.* **5,** 451–458
5. Löwe, J., and Amos, L. A. (1999) *EMBO J.* **18,** 2364–2371
6. Stricker, J., Maddox, P., Salmon, E. D., and Erickson HP. (2002). *Proc. Natl. Acad. Sci. U. S. A.* **99,** 3171–3175
7. Bi, E., and Lutkenhaus, J. (1991) *Nature* **354,** 161–164
8. Yu, X. C., and Margolin, W. (1997) *EMBO J.* **16,** 5455–5463
9. Mukherjee, A., and Lutkenhaus, J. (1998) *EMBO J.* **17,** 462–469
10. Mukherjee, A., and Lutkenhaus, J. (1999) *J. Bacteriol.* **181,** 823–832
11. Lu, C., Stricker, J., and Erickson, H. P. (1998) *Cell Motil. Cytoskel.* **40,** 71–86
12. Rivas, G., Lopez, A., Mingorance, J., Ferrandiz, M. J., Zorrilla, S., Minton, A. P., Vicente, M., and Andreu, J. M. (2000) *J. Biol. Chem.* **275,** 11740–11749
13. Hale, C. A., Rhee, A. C., and de Boer, P. A. (2000) *J. Bacteriol.* **182,** 5153–5166
14. Desai, A., and Mitchison, T. J. (1998) *Bioessays* **20,** 523–527
15. Romberg, L., Simon, M., and Erickson, H. P. (2001) *J. Biol. Chem.* **276,** 11743–11753
16. Mingorance, J, Rueda, S., Gomez-Puertas, P., Valencia, A., and Vicente, M. (2001) *Mol. Microbiol.* **41,** 83–91
17. Scheffers, D. J., and Driessen, A. J. (2002) *Mol. Microbiol.* **43,** 17–21
18. Erickson, H. P., Taylor, D. W., Taylor, K. A., and Bramhill, D. (1996) *Proc. Natl. Acad. Sci. U. S. A.* **93,** 519–523
19. Löwe, J., and Amos, L. A. (1998) *Nature.* **391,** 203–206
20. White, E. L., Ross, L. J., Reynolds, R. C., Seitz, L. E., Moore, G. D., and Borhani, D. W. (2000) *J. Bacteriol.* **182,** 4028–4034
21. Andreu, J. M., Oliva, M. A., and Monasterio, O. (2002) *J. Biol. Chem.* **277,** 43262–43270
22. Llorca O., Martin-Benito J., Grantham J., Ritco-Vonsovici M., Willison K. R., Carrascosa J. L., and Valpuesta J. M. (2001) *EMBO J.* **20,** 4065–4075
23. Diaz, J. F., Kralicek, A., Mingorance, J., Palacios, J. M., Vicente, M., and Andreu, J. M. (2001) *J. Biol. Chem.* **276,** 17307–17315
24. Löwe, J. (1998) *J. Struct. Biol.* **124,** 235–243
25. Diaz, J. F., and Andreu, J. M. (1993) *Biochemistry.* **32,** 2747–2755
26. Schmid, M. F., Dargahi, R., and Tam, M. W. (1993) *Ultramicroscopy* **48,** 251–264
27. Crowther, R. A., Henderson, R., and Smith, J. M. (1996) *J. Struct. Biol.* **116,** 9–16
28. Hardt, S., Wang, B., and Schmid, M. F. (1996) *J. Struct. Biol.* **116,** 68–70
29. Valpuesta, J. M., Carrascosa, J. L., and Henderson, R. (1994) *J. Mol. Biol.* **240,** 281–287
30. Marco, S., Chagoyen, M., de la Fraga, L. G., Carazo, J. M., and Carrascosa, J. L. (1996) *Ultramicroscopy* **66,** 5–10
31. Marabini, R., Masegosa, I. M., San Martín, C., Marco, S., Fernández, J. J., de la Fraga, L. G., Vaquerizo, C., and Carazo, J. M. (1996) *J. Struct. Biol.* **116,** 237–240
32. Jones, W. J., Leight, J. A., Mayer, F., Woese, C. R., and Wolfe, R. S. (1983) *Arch. Microbiol.* **136,** 254–261
33. Löwe, J., and Amos, L. A. (2000) *Biol. Chem.* **381,** 993–999
34. Wang, X., and Lutkenhaus, J. (1993) *Mol. Microbiol.* **9,** 435–442
35. Sossong, T. M., Jr., Brigham-Burke, M. R., Hensley, P., and Pearce, K. H., Jr. (1999) *Biochemistry* **38,** 14843–14850
36. Mukherjee, A., Dai, K., and Lutkenhaus, J. (1993) *Proc. Natl. Acad. Sci. U. S. A.* **90,** 1053–1057
37. Wang, X., and Lutkenhaus, J. (1996) *Mol. Microbiol.* **21,** 313–319
38. Caplow, M., Ruhlen, R. L., and Shanks, J. (1994) *J. Cell Biol.* **127,** 779–788
39. Lu, C., Stricker, J., and Erickson, H. P. (2001) *BMC Microbiol.* **1,** 7
40. Dai, K., Mukherjee, A., Xu, Y., and Lutkenhaus, J. (1994) *J. Bacteriol.* **176,** 130–136
41. Scheffers, D. J., de Wit, J. G., den Blaauwen, T., and Driessen, A. J. (2001). *FEBS Lett.* **494,** 34–37
42. Mukerjee, A., Saez, C., and Lutkenhaus, J. (2001) *Mol. Microbiol.* **183,** 7190–7197
43. Nogales, E. (2000) *Annu. Rev. Biochem.* **69,** 277–302
44. Feucht, A., Lucet, I., Yudkin, M. D., and Errington, J. (2001) *Mol. Microbiol.* **40,** 115–125
45. Gonzalez, J. M., Jimenez, M., Mingorance, J., Velez, M., Andreu, J. M., Vicente, M., and Rivas, G. (June 14, 2003) *J. Biol. Chem.* 10.1074/jbc.M305230200
46. Andreu, J. M., and Timasheff, S. N. (1986) *Methods Enzymol.* **130,** 47–59